



Legumain-induced intracerebrally crosslinked vesicles for suppressing efflux transport of Alzheimer's disease multi-drug nanosystem

Fuxin Jiang, Jian Ren, Yachai Gao, Jinna Wang, Yiping Zhao **, Fengying Dai *

School of Material Science and Engineering, Tianjin Key Laboratory of Separation Membranes and Membrane Processes, National Center for International Joint Research on Separation Membranes, Tiangong University, Tianjin, 300387, China

ARTICLE INFO

Keywords:

Legumain
Brain barrier
Efflux transport
Multi-drug delivery
Alzheimer's disease

ABSTRACT

Brain barrier is both a protective permeability hurdle and a limitation site where therapeutic agents are excluded to enter the target region. Designing drug vehicle to overcome this notorious barrier bottle is challenging. Herein, we construct a stimuli-responsive self-assembled nanovesicle that delivers water-soluble drugs to prevent the efflux transport of brain barriers by responding to the endogenously occurring signals in Alzheimer's disease (AD) brain microenvironment. Once stimuli-responsive vesicles are accumulated in intracerebrally, the intrinsically occurring legumain endopeptidase cleaves the Ac-Ala-Ala-Asn-Cys-Asp (AK) short peptide on the drug vesicles to expose the 1,2 thiol amino group to cyclize with the cyano groups on 2-cyano-6-aminobenzothiazole (CABT) of the chaperone vesicles, thus triggering the formation of cross-linked micrometre-scale vesicles. Such a structural alteration completely prevents further brain barriers efflux. The superior neuroprotective capacity of cross-linked vesicles is validated in senescence accelerated mouse prone 8 (SAMP8). This smart multi-drug delivery vesicle is promising to serve as a powerful system for AD treatment and can be adapted for the therapy of other central nervous system (CNS) disorders.

1. Introduction

No clinical treatment drug for Alzheimer's disease (AD) could completely reverse the aging process over the past decade. During these barren years, drug hunters were largely focused on identifying agents that target either β -amyloid, tau protein, metabolic disorder or neurotransmitters [1,2]. Although biologists have been struggling to pinpoint what really causes the disease, the more urgent clinical management dilemma is how to deliver sufficient dose of therapeutic drugs into brain parenchyma to avoid the continued deterioration of the medium and advanced patients. However, the disappointing fact is that about 98% of small molecule drugs and virtually all large molecule drugs failed to enter the brain due to the brain barrier [3–7].

Polymer vesicles nanomedicine presents a promising opportunity to greatly boost AD therapy [8–10]. Indeed, intensive investigations have demonstrated that functionalized vesicles can be employed as promising delivery systems to enhance loading of hydrophilic and hydrophobic drug and thus protect the drug from enzymatic degradation in blood [11]. Brain barrier could protect neuron against neurotoxin, but this barrier bring large difficulty for drug brain parenchyma retention. Efflux

pump distributed in the endothelial cell is emerging as a critical mechanism for nanomedicine brain efflux [12]. Higher brain endothelial cell internalization and exosmosis ratio of nanomedicine can be expected [13,14]. Yet, research results indicate that endothelial cell-penetrating properties of nanomedicine do not imply brain retention ability [15–17]. Targeting brain delivery does not solely increase penetration or suppress the efflux protein of BBB. The central mechanism by which modulate nanomedicine brain barrier transport and brain retention has been elucidated. Systems studies were performed to address the transport pathway, transport efficiency and thresholds for nanomedicine brain retention [18,19]. Indeed, nearly 75–95% of peak value nanomedicine that released in brain parenchyma was pushed out of the brain by efflux protein or paravascular glymphatic pathway [15,17,20–24]. The multimode overlay of influx and efflux BBB transport leading to the nanomedicine brain retention ratio raised at first, then decreased, and the peak appeared at 1–2 h after nanomedicine taken [15,17,21]. Therefore, drug targets delivery will be the strategies those can manage nanomedicine to overcome efflux in brain parenchyma.

The different environment of the diseased cell that provide a unique opportunity for rational design of nanomedicine. Numerous studies have

* Corresponding author.

** Corresponding author.

E-mail address: daifengying@tjpu.edu.cn (F. Dai).

<https://doi.org/10.1016/j.bioactmat.2020.11.024>

Received 22 July 2020; Received in revised form 7 November 2020; Accepted 13 November 2020

2452-199X/© 2020 The Authors. Production and hosting by Elsevier B.V. on behalf of KeAi Communications Co., Ltd. This is an open access article under the CC

BY-NC-ND license (<http://creativecommons.org/licenses/by-nc-nd/4.0/>).

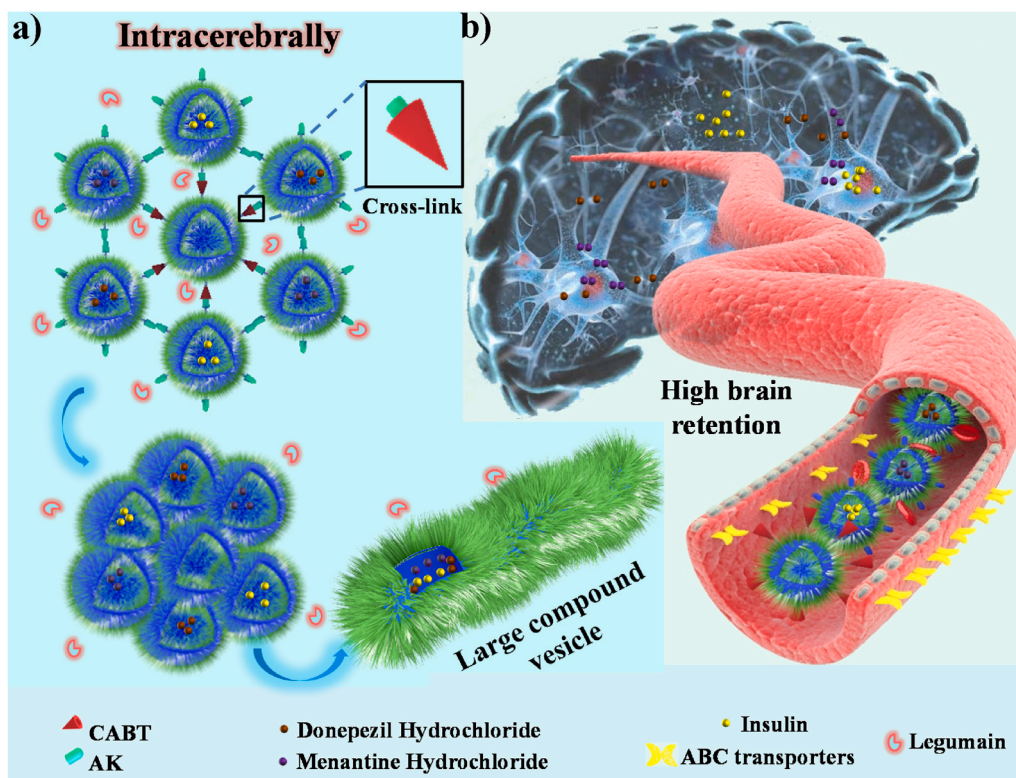


Fig. 1. Schematic diagram of brain response. a) Responsive cross-linked of large compound vesicles formed in intracerebrally. b) Inhibition of brain barrier efflux and synergistic treatment of AD.

demonstrated that legumain has prominent role in AD pathogenesis, which has major clinical implications [25]. During ageing and other cellular stressors in the AD brain, legumain translocates from the endolysosome into the cytoplasmic space, and then legumain is widely distributed in brain parenchyma in AD patients but is not activated in CSF [26–28]. These understanding of the active legumain and nanomedicine efflux mechanism that control brain retention, revealing the crucial role of reprogramming factors of legumain for target retention AD brain [29–31].

We hypothesize that legumain could be selected as a target to trigger in situ cross-linking of small size nanodrug particles to form large sized drug clusters and thus block the efflux of brain. Thus, three types of smart size switchable polymer vesicles loaded respectively with insulin, donepezil hydrochloride and memantine hydrochloride were designed and fabricated in this study. Among them, the insulin (INS) drug is used to down-regulate insulin resistance, and donepezil hydrochloride (DON HCl) is used to inhibit the breakdown of intracellular acetylcholine to maintain stable cholinergic content. Memantine hydrochloride (MEM HCl) is expected to reduce excitatory amino acid toxicity and prevent synaptic dysfunction caused by Ca^{2+} influx [32–36]. The mixture of the V_{INS} , V_{DON} , V_{MEM} vesicles and V_{CABT} vesicles was named MEM/DON/INS ICV. When intrinsically legumain endopeptidase cleaves the Ac-Ala-Ala-Asn-Cys-Asp (AK) short peptide on surface of the (V_{INS} , V_{DON} , V_{MEM}) vesicles, then the exposure 1,2 thiol amino group could cyclize with the cyano group of 2-cyano-6-aminobenzothiazole (CABT) and thus triggering the formation of cross-linked vesicles, which could inhibit the brain efflux (Fig. 1a and b). These intelligent nanovesicles provide the possibility for synchronous delivery of different drugs that are precisely regulated to improve mitochondrial and synaptic functions from different mechanisms in neuronal cells. It is anticipated that this smart system could also enhance the brain retention of drugs, collectively improving the memory ability of AD patients.

2. Experimental section

2.1. Materials

Sn(II)2-ethylhexanoate ($\text{Sn}(\text{Oct})_2$) and $\epsilon\text{-CL}$ were purchased from aladdin (Shanghai, China). Dextran was purchased from Yeasen Biotech Co., Ltd (Shanghai, China). N, N-dimethylformamide (DMF), dichloromethane (CH_2Cl_2), Dimethyl sulfoxide (DMSO) and triethylamine (Et_3N) were all purchased from KGM chemical reagent (Tianjin, China). 2-hydroxyethyl 2-bromoisobutyrate (HEBIB), N,N,N',N',N'-pentamethyldiethylenetriamine (PMDETA), acryloyl chloride and CuBr were purchased from HEOWNS (Tianjin, China). The $\text{A}\beta_{1-42}$ and 1, 1, 1, 3, 3, 3-hexafluoro-2-propanol (HFIP) were purchased from GL Biochem (Shanghai, China). 2-Cyano-6-aminobenzothiazole (CABT) was purchased by Shanghai Chemical Pharm-Intermediate Tech. Co., Ltd (Shanghai, China). The 4% paraformaldehyde (PFA), 3-(4,5-dimethylthiazol-2-yl)-2,5-diphenyltetrazolium bromide (MTT), poly (vinylidene fluoride) (PVDF) membrane, rhodamine B (RhB), Nissl staining solution, 2-(2-hydroxyethyl)-1-piperazinyl ethanesulfonic acid (HEPES), Hoechst 33258, 4',6-diamidino-2-phenylindole (DAPI), and postsynaptic density protein-95 (PSD-95) rabbit monoclonal antibody (AF1096), protein kinase B (Akt) mouse monoclonal antibody (AF0045), Akt rabbit monoclonal antibody (AF1777), anti-NeuN antibody (AF1072), anti-rabbit secondary antibody (A0453) and anti-mouse secondary antibody (A0428) were purchased from Beyotime Biotechnology (Shanghai, China). Memantine hydrochloride (MEM HCl), donepezil hydrochloride (DON HCl) and insulin (INS) were all purchased from Xiensi Biochemical Technology Co., Ltd (Nanjing, China). AK peptide (Ac-Ala-Ala-Asn-Cys-Asp) was customized by PHTD peptide Co., Ltd (Zhengzhou, China). Malondialdehyde (MDA) detection kit, esterase enzyme, DMEM (high glucose), fetal bovine serum (FBS), the acetylcholinesterase (AChE) detection kit, 3, 3'-diaminobenzidine (DAB), hematoxylin eosin (HE), and nickel ammonium were purchased

from the Jiancheng Bioengineering Institute (Nanjing, China). 3D MAX 2013 was used for preparing Fig. 1.

2.2. Synthesis of the PCL-HEBIB macroinitiator

Briefly, 2-hydroxyethyl 2-bromoisoobutyrate (HEBIB, 0.1 g, 0.47 mmol) and anhydrous ϵ -caprolactone (2.32 g, 20.2 mmol) were dissolved in refined toluene (6 mL) in a 25 mL flask and Sn(Oct)₂ (200 μ L) were used as catalysts. The flask was then sealed and placed in an oil bath at 110 °C. The molar ratio of HEBIB/ ϵ -CL was 1:45. After 12 h of polymerization, the reaction was terminated by exposure to air. The residue was dissolved in dichloromethane, precipitated from cold ethyl ether three times. After drying overnight in vacuum, the product was obtained with 85% yield and named PCL-HEBIB. A series of products were synthesized by varying the molar ratio of ϵ -CL/HEBIB.

2.3. Preparation of dextran-acryloyl chloride (Dextran-AC) macromonomer

Dextran (Mw = 2,000, 0.8 g, 4.9 mmol of anhydroglucose unit) was dissolved in N,N-dimethylformamide (DMF, 20 mL) and stirred at 0 °C, at the same time, triethylamine (Et₃N, 50 μ L) was added. Then, dichloromethane (8 mL) and acryloyl chloride (32 μ L, 0.4 mmol) were mixed and slowly added dropwise to the flask. After 2 h, the flask was sealed at room temperature for 24 h. The mixture was thoroughly dialyzed against distilled water (MWCO: 1000 Da) for 72 h. After lyophilization, the product was obtained as a white solid with 77% yield and named Dextran-AC.

2.4. Synthesis of PCL-Dextran (PCL-Dex) copolymer

In a typical procedure, PCL-HEBIB (0.2 g), Dextran-AC (0.4 g) and CuBr (5.7 mg, 0.04 mmol) were dissolved in refined dimethyl sulfoxide (DMSO, 8 mL) in a 25 mL reaction tube. The mixture was repeated freezing and thawing three times. N, N, N', N, 'N'-pentamethyldiethylenetriamine (PMDETA, 6.9 mg, 0.04 mmol) was then dissolved in refined DMSO (0.5 mL) and added followed by freezing and thawing for another 3 times. The polymerization was carried out in an oil bath at 70 °C for 6 h. The resulting polymer was washed 5 times with ultrapure water to remove water-soluble compounds, and then dialyzed for 72 h (MWCO: 3500 Da). After lyophilization, the product was obtained as a white solid with 80% yield and named PCL-Dextran (PCL-Dex). Similarly, a series of PCL_n-Dex were obtained by changing the molar ratio of PCL-HEBIB/Dextran-AC.

2.5. Synthesis of PCL-Dex-PGMA

Similarly, PCL-Dex (0.56 g, 0.045 mmol), glycidyl methacrylate (GMA, 0.16 g, 0.113 mmol) and CuBr (6.5 mg, 0.045 mmol) were dissolved in refined anhydrous DMSO (10 mL) in a 25 mL reaction tube. After freezing and thawing, PMDETA (7.8 mg, 0.045 mmol) was then dissolved in anhydrous DMSO (0.4 mL) and added. The resulting polymer was thoroughly dialyzed and lyophilized overnight in vacuum, the product was obtained and named PCL-Dex-PGMA.

2.6. Synthesis of PCL₄₅-Dex₆₀-PGMA₁₂-AK and PCL₄₅-Dex₆₀-PGMA₁₂-CABT

PCL₄₅-Dex₆₀-PGMA₁₂ (100 mg) and AK peptide (Ac-Ala-Ala-Asn-Cys-Asp) (5 mg) were dissolved in DMSO (5 mL) and continuously stirred at 25 °C for 24 h. Then, the mixture was thoroughly dialyzed against distilled water (MWCO: 3500 Da) for 72 h, and then lyophilized. PCL₄₅-Dex₆₀-PGMA₁₂-CABT was successfully synthesized by adopting the same operation.

2.7. Preparation of PCL_n-Dex₆₀ nanoparticles

PCL_n-Dex₆₀ (10 mg) copolymer was dissolved in DMSO (2 mL) and allowed to dissolve completely by sonication. Then, the PCL_n-Dex₆₀ solution was slowly added to 10 mL Milli-Q water, and stirred 12 h at 25 °C. The mixture was thoroughly dialyzed against distilled water (MWCO: 1000 Da) for 72 h. Similarly, the nanoparticles of PCL₄₅-Dex₆₀-PGMA₁₂, PCL₄₅-Dex₆₀-PGMA₁₂-AK and PCL₄₅-Dex₆₀-PGMA₁₂-CABT were successfully prepared.

2.8. Polymers and nanoparticles characterization

The chemistry structures were examined by ¹H NMR (AVANCE 400 MHz, Bruker AXS Inc, Madison, Wisconsin). The hydrodynamic diameter was carried out with a Malvern Zetasizer nano ZS apparatus (Malvern Instruments, Malvern, USA). Nanoparticles were diluted with demineralized water, added onto copper grids and dried, then stained with uranyl acetate (0.2 wt%), and visualized using a Hitachi H-600 (Chiyoda, Tokyo, Japan) transmission electron microscope (TEM) operating at 200 kV.

2.9. Static light scattering (SLS) of PCL₄₅-Dex₆₀ nanoparticles

Static light scattering (SLS) technique was employed to analyze the vesicular structure of the PCL₄₅-Dex₆₀ polymer assemblies. The SLS data for PCL₄₅-Dex₆₀ in water at 25.0 ± 0.1 °C was carried out and the intensity of scattered light at different angle was plotted against q², where q is scattering vector magnitude (Guinier plot) [37,38].

Note: In SLS experiment, intensity was measured as a function of q (which was varied by angle θ). The variable q represents the scattering vector magnitude. It is given by the equation:

$$q = \frac{4\pi n \sin\left(\frac{\theta}{2}\right)}{\lambda_0} \quad (1)$$

Here n is the solution refractive index (1.332) and λ_0 is the incident wavelength, ie: 632.8 nm. The radius of gyration (R_g) was calculated by the equation:

$$\ln(I(q)) = \ln(I(0)) - \frac{q^2 R_g^2}{3} \quad (2)$$

Here slope of the graph is $R_g^2/3$. In the case of PCL₄₅-Dex₆₀, Slope = 3340.4. So $R_g = 100.1$ nm.

2.10. Characterization of legumain induced aggregation of PCL₄₅-Dex₆₀-PGMA₁₂-AK nanovesicles and PCL₄₅-Dex₆₀-PGMA₁₂-CABT nanovesicles

At the molar ratio of 1:1, 3:1, 5:1, 7:1, PCL₄₅-Dex₆₀-PGMA₁₂-AK nanovesicles and PCL₄₅-Dex₆₀-PGMA₁₂-CABT nanovesicles with 5 μ L legumain (0.5 mg mL⁻¹) were incubated in 2-(2-hydroxyethyl)-1-piperazinyl ethanesulfonic acid (HEPES) buffer (pH = 5.5) for 6 h. The hydrodynamic diameter of cross-linked nanoparticles was determined by DLS analysis. At the same time, TEM images of cross-linked nanoparticles incubated with legumain for 6 h were observed at 200 kV using Hitachi H-600 (Japan).

2.11. Preparation of drug encapsulated vesicles

Typically, donepezil hydrochloride (5 mg) and PCL₄₅-Dex₆₀-PGMA₁₂-AK polymer (20 mg) were dissolved in DMSO (2 mL) and slowly added to 10 mL Milli-Q water at a rate of 10 μ L s⁻¹. The resulting solution was stirred for 8 h, dialyzed against Milli-Q water (MWCO: 3,500Da) for 48 h, named V_{DON} and then lyophilized. The insulin-loaded vesicles (V_{INS}) and memantine hydrochloride-loaded vesicles (V_{MEM}) were prepared by the same operation. The freeze-dried V_{DON} or V_{INS} or V_{MEM} (1 mg) was dissolved in DMSO (1 mL), respectively, diluted to 30

times, and the absorbance at 270, 276 and 365 nm was measured on a UV-1901 spectrophotometer (China).

$$\text{Drug loading content (DLC)} = \frac{\text{weight of drug in nanovesicle}}{\text{weight of nanovesicle}} \times 100\% \quad (3)$$

Similarly, $\text{RhB}^{\text{Vesicle}}_{\text{AK}}$ was successfully prepared.

2.12. In vitro drug release studies

The V_{DON} or V_{INS} or V_{MEM} vesicles (3 mL, 2 mg mL⁻¹) were taken in a dialysis bag (MWCO = 10,000 Da), respectively, and they were immersed in phosphate buffer saline (PBS, pH = 7.4, 97 mL) at 37 °C, then 10 units of enzyme were added and dialyzed with constant stirring [39,40]. At specific time intervals, 4.0 mL of the dialysate was withdrawn and replaced with an equal volume of fresh PBS buffer. The amount of drug released in each aliquot was measured by using absorption spectroscopy to quantify their percentage of cumulative release. The cumulative release rate of the drug in MEM/DON/INS ICV large nanoaggregates were detected with the same way.

2.13. Cell lines and animals

Human neuroblastoma cells (SH-SY5Y) and Red blood cell were purchased from Cell Bank of Chinese Academy of Sciences. Normal male aging mouse (Senescence accelerated-resistant mouse 1, SAMR1) and rapid male aging mouse (SAMP8) mice were purchased from Animal Breeding Center of the First Affiliated Hospital of Tianjin University of Traditional Chinese Medicine.

2.14. Preparation of A β 42 aggregates

A β ₁₋₄₂ lyophilized powder and 300 μ L 1, 1, 1, 3, 3, 3-hexafluoro-2-propanol (HFIP) were injected into the reagent bottle and vortex. After mixing, it was allowed to stand at room temperature to obtain an A β -HFIP solution (1 mM). Prior to use, a small amount of DMSO was used for sonication, and PBS buffer was added and incubated for 1 week. The solution was diluted to the target concentration gradient with serum-free DMEM medium to used follow-up test.

2.15. Cell damage model

SH-SY5Y cells were maintained in DMEM medium, containing 10% fetal bovine serum (FBS) under the culture conditions of 5% CO₂ and 37 °C. Cells were harvested from flasks and plated in 96-well polystyrene plates with approximately 10⁴ cells per well. Plates were incubated at 37 °C for 24 h to allow the cells to attach, followed by introduction of A β 42 = 5 μ M/well, 10 μ M/well, 15 μ M/well, 20 μ M/well, 25 μ M/well, respectively. After 6, 12, 24, 48 h, the cells were treated with 5 μ L MTT solution (10 mg mL⁻¹) for 4 h and then 100 μ L DMSO was added to each well. Plates were shaken at room temperature for 10 min to dissolve the crystals before the absorbance at 490 nm was measured using a Variskan LUX (Thermo Scientific, USA). Averages of six replicate wells were used for each sample.

2.16. Protective effect of treatment group on A β 42-injured SH-SY5Y cells

MV was the mixture of the V_{INS} , V_{DON} and V_{MEM} vesicles. ICV was the mixture of the V_{INS} , V_{DON} , V_{MEM} vesicles and V_{CABT} vesicles, those could be induced cross-linking by over-activated legumain. "MEM/DON/INS V" means three drugs co-encapsulation vesicle. Similarly, SH-SY5Y Cells were transferred to 96-well polystyrene plates and incubated at 37 °C for 24 h to allow the cells to attach, followed by introduction of A β 42 = 15 μ M/well, DMEM = 150 μ L/well, DON HCl = 15 μ L/well, MEM HCl = 15 μ L/well, INS = 15 μ L/well, DON/MEM MV = 15 μ L/well, DON/MEM ICV = 15 μ L/well, INS/MEM MV = 15 μ L/well, INS/MEM ICV = 15 μ L/well,

well, DON/INS MV = 15 μ L/well, DON/INS ICV = 15 μ L/well, MEM/DON/INS MV = 15 μ L/well, MEM/DON/INS V = 15 μ L/well, MEM/DON/INS ICV = 15 μ L/well, respectively, and the concentration of each drug is about 0.04 mg mL⁻¹ DMEM medium. After culture for 48 h at 37 °C, the MTT experiment was carried out in accordance with the above procedure.

2.17. Retention of RhB^{ICV} and $\text{RhB}^{\text{Vesicle}}_{\text{AK}}$ vesicles in SH-SY5Y cell by laser scanning confocal microscope (LSCM)

SH-SY5Y cells were transferred to laser confocal dish and incubated in DMEM. The induced cross-linked vesicles (RhB^{ICV} , the mixture of $\text{RhB}^{\text{Vesicle}}_{\text{AK}}$ and V_{CABT} vesicles) or noncross-linked Vesicle_{AK} ($\text{RhB}^{\text{Vesicle}}_{\text{AK}}$) were added to the medium at a final concentration of 0.2 mg mL⁻¹. After 2 h and 24 h incubation, SH-SY5Y cells were washed with PBS three times and fixed with 4% paraformaldehyde in PBS for 15 min at 37 °C, then stained with Hoechst 33258 (400 μ L, 10 μ g mL⁻¹) to allow nuclear staining or LysoTracker Green (300 nM) to allow lysosome staining. Images of cells were taken with Nikon A1 Laser scanning confocal microscope (Japan).

2.18. Internalization of RhB^{ICV} and $\text{RhB}^{\text{Vesicle}}_{\text{AK}}$ nanovesicles by SH-SY5Y cells

SH-SY5Y cells were transferred to 6-well polystyrene plates with approximately 10⁵ cells per well. RhB^{ICV} or $\text{RhB}^{\text{Vesicle}}_{\text{AK}}$ was added at the above concentrations. After 2 h, 8 h and 24 h incubation, the SH-SY5Y cells were trypsinized and centrifuged at 1000 r minutes⁻¹ for 5 min and washed 3 times with PBS. Then, single cells were resuspended in PBS (200 μ L) and tested on a BD Calibur flow cytometer (BD Biosciences, Bedford, MA).

2.19. Red blood cell aggregation

The red blood cells were transferred to 6-well polystyrene plates with approximately 10⁵ cells per well, and then 0.2 mL distilled water, 0.2 mL saline, 0.2 mL diluted MEM/DON/INS MV solution (1:5 saline), 0.2 mL diluted MEM/DON/INS ICV solution (1:5 saline) were added into the solution of well, respectively. After culture for 1 h at 37 °C, the images were observed by microscope.

2.20. Animal treatment

SAMR1 littermate mice and SAMP8 littermate mice (male, 7 months of age, 28–32 g) were maintained at 23 ± 2 °C and 30 ± 8% in the animal room. All animal procedures were performed in accordance with the Guidelines for Care and Use of Laboratory Animals of Tiangong University and approved by the Animal Ethics Committee of Beijing Municipal Science & Technology.

The mice were divided into 8 groups: SAMR1 normal group (n = 6), SAMP8 saline group (n = 6), and naked drug (the mixture of MEM/DON/INS) treated SAMP8 mice group (n = 6 for each group), DON/INS MV treated SAMP8 mice group (n = 6), DON/INS ICV treated SAMP8 mice group (n = 6), MEM/DON/INS MV treat SAMP8 mice group (n = 6), MEM/DON/INS V treated SAMP8 mice group (n = 6) and MEM/DON/INS ICV treated SAMP8 mice group (n = 6). Mice of each group were administered nasally for 24 days at the dose of MEM was 0.033 mg drug/kg body weight/day, the dose of DON was 0.033 mg drug/kg body weight/day and the dose of INS was 0.9 IU/kg body weight/day. Then, the Morris water maze (MWM) was performed for mice learning and memory test.

2.21. Morris water maze (MWM)

The mice were tested in a water maze (1.3 m in diameter, temperature was maintained at 24 ± 1 °C). The platform (diameter of 15 cm)

was fixed to beneath the water surface during the training period. Each subject was given 4 trials/day from different quadrants for 5 consecutive days with a 15-min intertrial interval. The maximum trial length was 60 s and if the mice could not find the platform within 60s, they were manually guided to catch the target platform. The trajectory of each mouse was recorded and analyzed for latency and swim speed. At 24 h after the last learning trial, a probe trial was presented during which time the platform was removed and the percentage of time spent in the quadrant, which previously contained the escape platform during task acquisition was measured over 60 s [25].

2.22. Western blot (WB)

Animals were euthanized, the hippocampus tissue of the SAMP8 mice was obtained. This tissue was thoroughly ground and centrifuged in the lysis buffer. An equal amount of protein sample (30 µg/sample) was processed at 97 °C for 6 min, centrifuge and transfer to film at room temperature. The poly (vinylidene fluoride) (PVDF) membrane was placed in a blocking solution (TBST/5% skim milk powder) and blocked at room temperature for 30 min. Primary antibody that diluted with blocking solution was added and incubated for 60 min at room temperature. After the 1×TBST washed, an appropriately diluted secondary antibody was added and incubated for 60 min. The development operation was carried out after rinsed 3 times with 1×TBST. The analysis was performed using Quantity one software, and the ratio of the control well (first well)/tubulin was taken as 1.

2.23. Malondialdehyde (MDA) content

According to the above method, the hippocampus was weighed, and 9 times volumes of physiological saline were added. The tissue was mechanically homogenized in an ice water bath condition, centrifuged at 2500 r minutes⁻¹ for 10 min, and the supernatant was taken for testing. After the addition of the MDA detection reagent, it was vortexed and placed in a boiling water bath for 30 min. The absorbance values of the supernatants at 532 nm were measured under UV-1901 spectrophotometer (China).

2.24. Acetylcholinesterase (AChE) activity

The tissue was treated in the same way, after AChE kit was added, and reacted accurately at 37 °C for 6 min. The absorbance values of the supernatants at 412 nm were measured under UV-1901 spectrophotometer (China).

2.25. Immunofluorescence

Animals were euthanized, the whole brain was harvested and fixed in 4% paraformaldehyde (PFA), then cut into hippocampus slices. Briefly, hippocampus slices were incubated for 2 h in a 1:1000 dilution of PSD-95 rabbit monoclonal antibody and reacted for 2 h in Akt mouse monoclonal antibody solution (1:1000 dilution), then immersed in fluorescence secondary antibody solution (1:500 dilution) for 1 h. Cell nuclei were labeled using 4',6-diamidino-2-phenylindole (DAPI) for 10 min. These sections were observed under Nikon A1 Laser scanning confocal microscope (Japan).

2.26. NeuN staining and nissl staining

According to the above method, the thin hippocampus slice was incubated with anti-NeuN antibody diluted appropriately for staining 12 h at 4 °C. After washing, the slice was treated with secondary antibody for 35 min at room temperature and then exposed to 3,3'-diaminobenzidine (DAB) to produce the chromogenic reaction. Similarly, nissl stained sections were prepared. The stained hippocampus slice was observed by Olympus CX41 microscope (Japan), and the NeuN positive

cell numbers in the hippocampus were analyzed using ImageJ.

2.27. Hematoxylin eosin (HE) staining

Similarly, after the mice were sacrificed, the heart, liver, spleen, lungs, and kidneys were fixed and sliced. The sections were deparaffinized, washed in distilled water and incubated for 5 min in hematoxylin solution. Excess hematoxylin solution was washed away with running tap water and hydrochloric acid ethanol. The sections were then counterstained in an eosin solution for 3–4 min, washed in running tap water, dehydrated by graded alcohol, and fixed with a neutral resin. The pathological changes of the tissue were observed at 100X under an Olympus CX41 microscope (Japan).

2.28. Brain retention

The induced cross-linked vesicles (^{RhB}ICV) or noncross-linked Vesicle_{AK} (^{RhB}Vesicle_{AK}) (40 µL) were injected into the SAMP8 mice by nasal administration, and ex vivo tissue imaging was performed at the indicated of 2 h and 12 h by KODAK In-Vivo Imaging System FX Pro (USA).

2.29. DON HCl content determination in the brain

MEM/DON/INS MV and MEM/DON/INS ICV were nasal administration at an equivalent dose of 40 µL of SAMP8 mouse (n = 3 per group). After 24 h, the mice were sacrificed and washed with cold saline. The brain was weighed and dissolved in a hexane-diethyl ether solution (1:1). The mixed solution was vortexed and centrifuged, and the upper organic phase was dried under nitrogen. After reconstitution with 0.2 mL of methanol, the concentration of DON HCl was determined by LC-MS (Agilent 1290–6460). The content is calculated according to the formula :

$$W = \frac{C \cdot V \cdot N}{m} \quad (4)$$

In the formula:

- W — the content of the target in the sample, in milligrams per kilogram (mg kg⁻¹)
- C — the concentration of the target in the sample determination solution (mg L⁻¹)
- V — Constant volume (mL)
- N — dilution factor
- m — the sample quality of the sample in grams (g).

2.30. Hemolysis ratio

The 10 mL tubes were divided 8 groups: followed by introduction of 2.5 mL distilled water (positive controls), 2.5 mL saline (negative controls), 2.4 mL saline + 0.1 mL (MEM/DON/INS MV solution), 2.4 mL saline + 0.1 mL (MEM/DON/INS ICV solution), 2.3 mL saline + 0.2 mL (MEM/DON/INS MV solution), 2.3 mL saline + 0.2 mL (MEM/DON/INS ICV solution), 2.2 mL saline + 0.3 mL (MEM/DON/INS MV solution), 2.2 mL normal saline + 0.3 mL (MEM/DON/INS ICV solution), respectively. The diluted blood (anticoagulant blood with 2% potassium oxalate 4:5 normal saline) was successively added into the solution of all groups. After incubation at 37 °C for 60 min, the blended liquid was centrifuged at 1000 rpm for 5 min. The supernatants were transferred into the 96-well plates, and the optical density (OD) values were measured at 545 nm with a microplate reader.

Hemolysis ratio = (Samples-negative controls) / (positive controls - negative controls) * 100%.

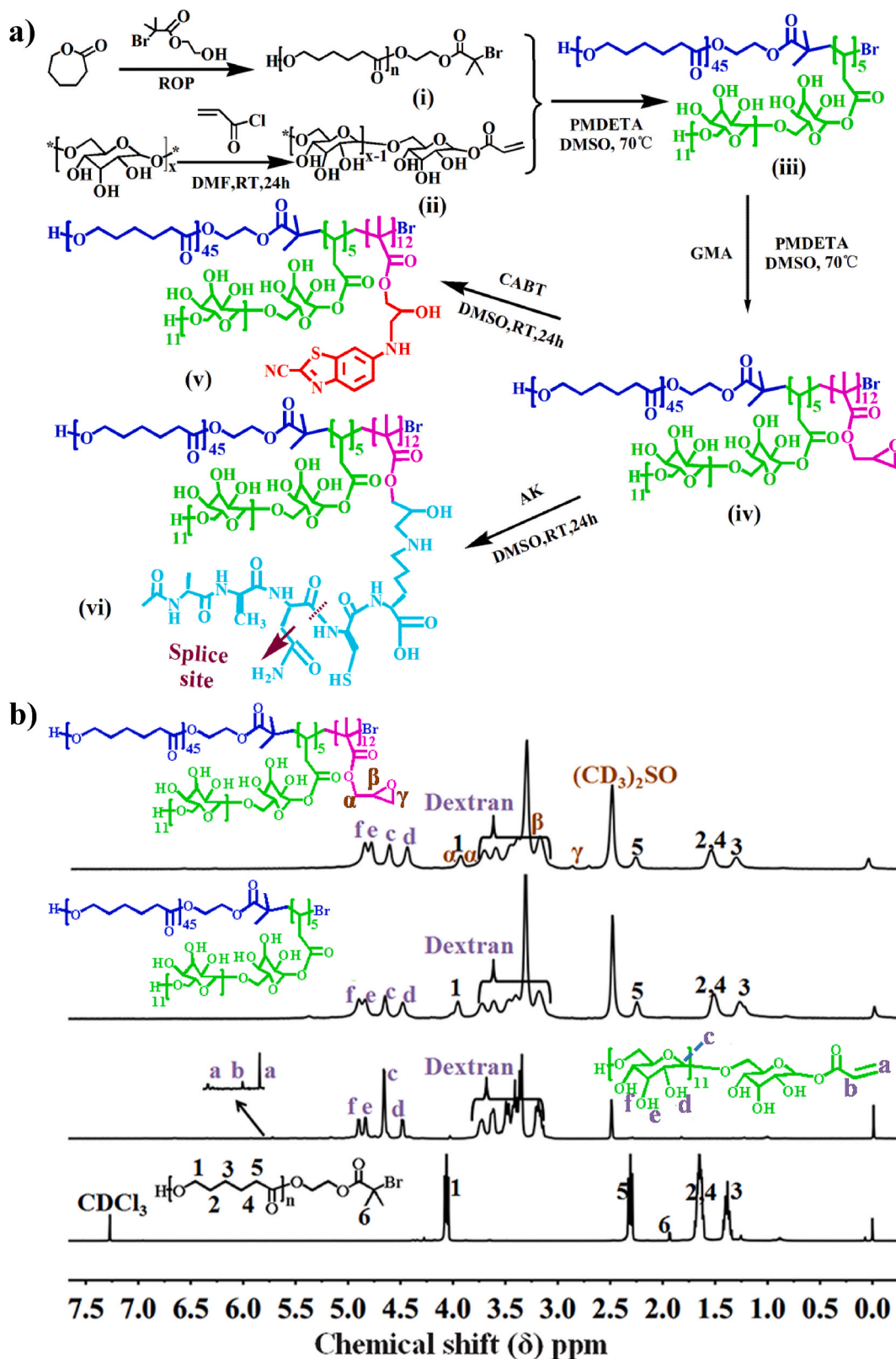


Fig. 2. Synthesis route and characterization of polymers. a) The synthetic route of PCL-HEBIB (i), Dex-AC (ii), PCL-Dex (iii), PCL-Dex-PGMA (iv), PCL-Dex-PGMA-CABT (v) and PCL-Dex-PGMA-AK (vi). b) ^1H NMR spectra of the PCL-HEBIB, Dex-AC, PCL-Dex and PCL-Dex-PGMA.

2.31. Determination of blood biochemical indicators

After the MWM experiment, the blood was collected from the orbital venous plexus of mice, and the serum was separated by centrifugation.

The serum alanine aminotransferase (ALT), aspartate aminotransferase (AST), alkaline phosphatase (ALP), and creatinine (CREA), serum urea (UREA), uric acid (UA) were determined by an automatic biochemical analyzer.

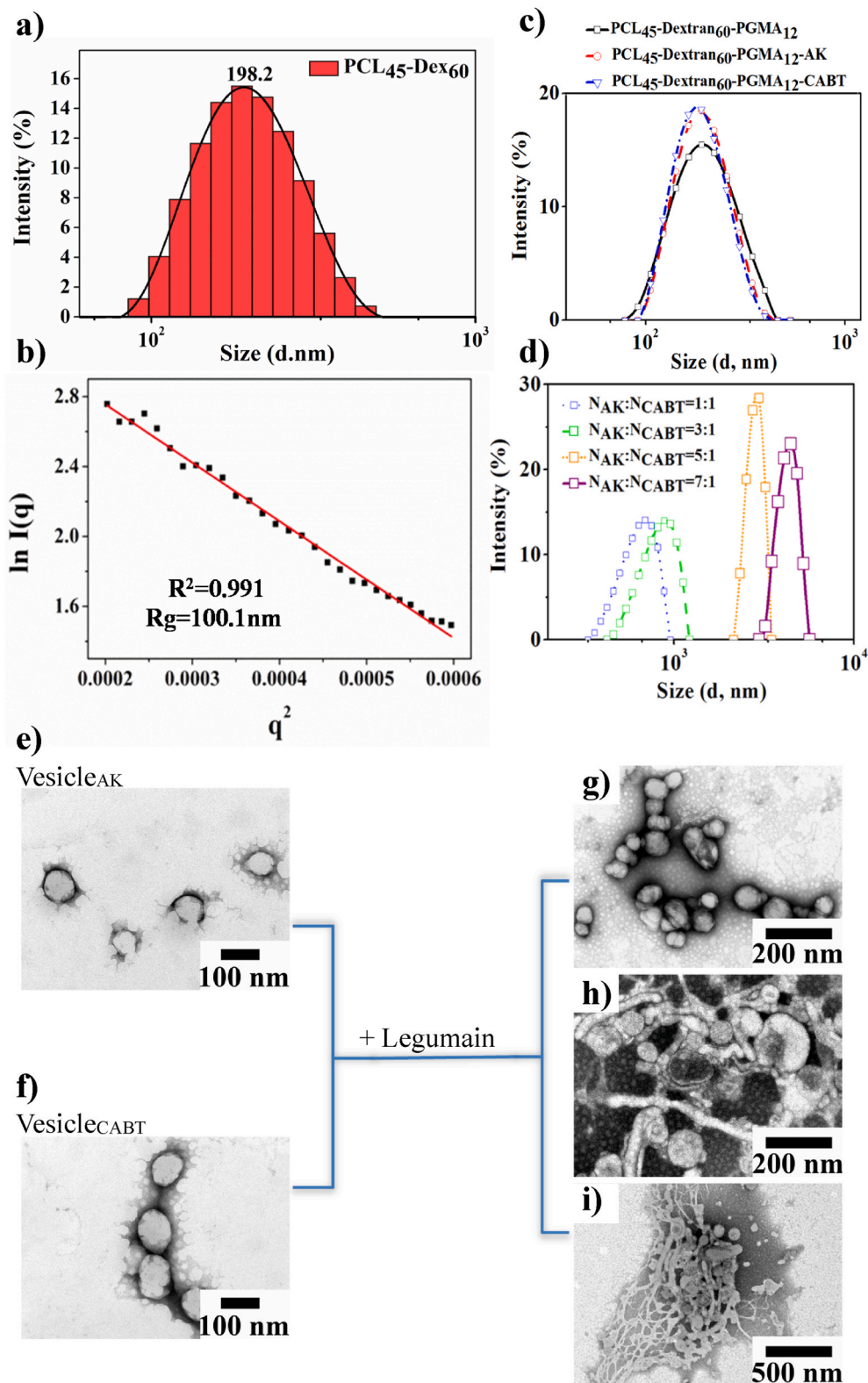


Fig. 3. Polymer self-assembled vesicles and legumain induced cross-linked vesicle. a) The hydrodynamic diameter of PCL₄₅-Dex₆₀ and b) Noncross-linked nanoparticles. b) Static light scattering data for PCL₄₅-Dex₆₀ in PBS at 25 °C. The hydrodynamic diameter of c) Noncross-linked nanoparticles and d) Legumain-induced cross-linked nanoparticles. TEM images of e) PCL₄₅-Dex₆₀-PGMA₁₂-AK, f) PCL₄₅-Dex₆₀-PGMA₁₂-CABT nanoparticles and cross-linked nanoparticles at molar ratio of [Vesicle_{AK}]/[Vesicle_{CABT}] = g) 1:1, h) 3:1, i) 5:1.

2.32. Statistical analysis

Statistical analyses for in vitro and in vivo experiments were performed by using Origin. The significance level was set at *P < 0.05, **P < 0.01, ***P < 0.005. Error bars represent the standard deviation of the mean (±SD), and P values were indicated in the figure captions and main text.

3. Results and discussion

3.1. Preparation and characterization of induced cross-linked vesicles

In order to obtain the vesicle via self-assemble of macromolecules, we designed a graft amphiphilic copolymer. The poly(ε-caprolactone) (PCL) based brush-like polymer is special for its unique side-chain crystallization

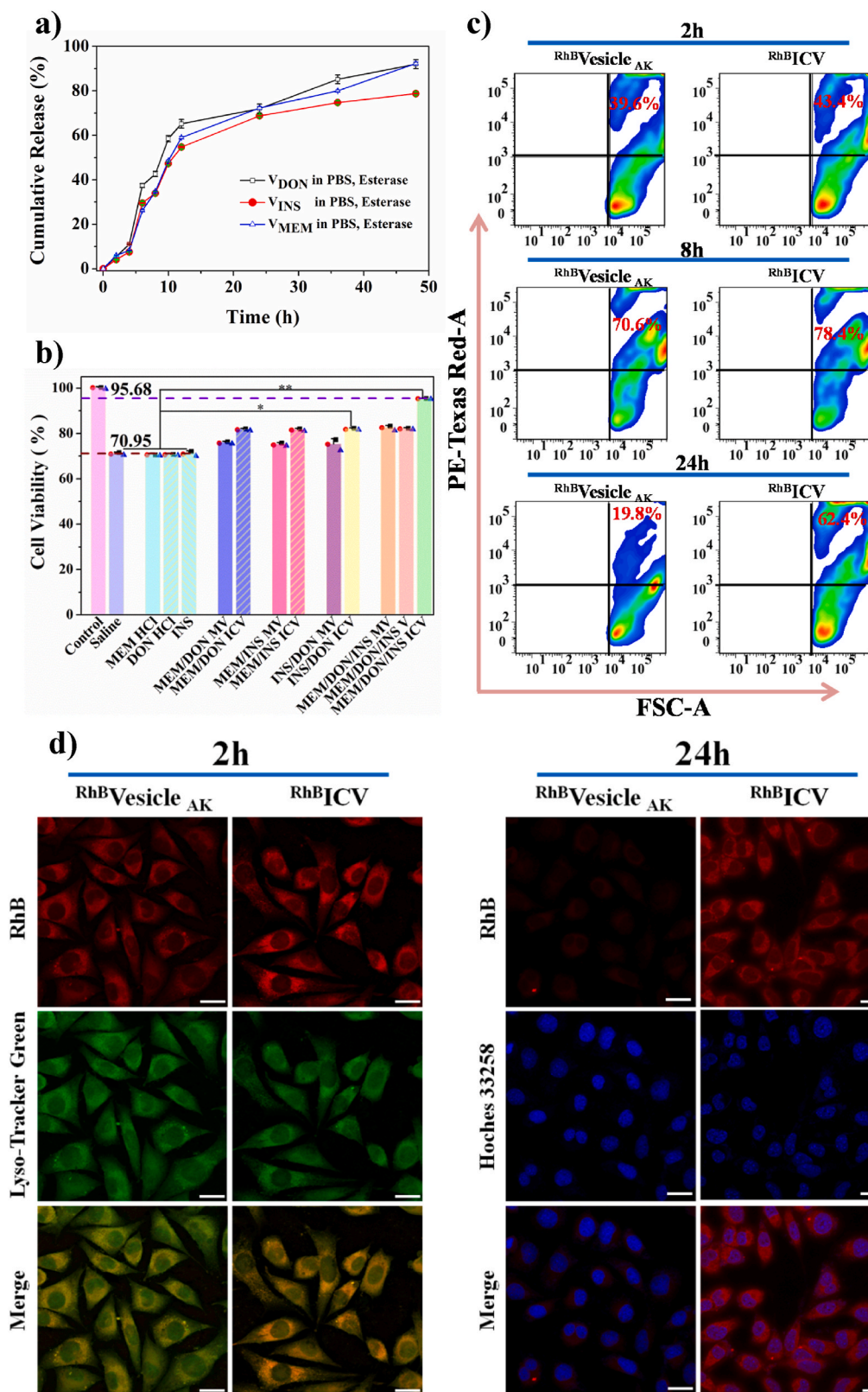


Fig. 4. Legumain-induced cross-linked vesicles can effectively protect SH-SY5Y from A β -caused damage by improving the retention efficiency of intracellular drugs. a) Cumulative drug release of Vesicle_{DON}, Vesicle_{INS} and Vesicle_{MEM} in the presence of esterase enzyme. b) The protective effect of drug-loaded vesicles on the cytotoxicity of A β -induced SH-SY5Y cells (mixing vesicles (MV), induced cross-linked vesicles (ICV), three drugs encapsulated in the same vesicles (MEM/DON/INS V)). c) Typical flow cytometry data of SH-SY5Y cells after incubation with Rh^BVesicle_{AK} or Rh^BICV at DMEM for 2 h, 8 h and 24 h. d) LCMS images of SY5Y cells incubated with Rh^BVesicle_{AK} or Rh^BICV at DMEM for 2 h or 24 h (Scale bar, 50 μ m). The mean \pm SD is shown. *p < 0.05, **p < 0.01 and ***p < 0.005 (n = 3) versus control.

phenomenon which is beneficial for the formation of an intermediate hydrophobic layer of vesicle. More importantly, the grafted hydrophilic dextran (Dex) branches contain a large number of hydroxyl groups, which would facilitate the formation of stable inner and outer hydrophilic layers of vesicles [41]. With the dual-modal driving force of

hydrophilic/hydrophobic interaction, polycaprolactone-dextran (PCL-Dex) vesicles are more likely to be formed. Herein, we developed a brush-like copolymer composed of biodegradable hydrophobic PCL and poly(glycidyl methacrylate) (PGMA) that containing active epoxy group for the conjugation of legumain-cleavable peptide Ac-Ala-Ala-Asn-Cys-Asp (AK).

The preparation route of the polycaprolactone-dextran-poly(glycidyl methacrylate)-AK (PCL-Dex-PGMA-AK) was depicted in Fig. 2a. Similarly, the chaperone PCL-Dex-PGMA-2-cyano-6-aminobenzothiazole (PCL-Dex-PGMA-CABT) brush copolymer for the brain in situ crosslinked reaction was also synthesized. The chemical compositions of the obtained polymers were confirmed by ^1H NMR spectra (Fig. 2b), where the features bands were present: $\delta = 5.8\text{--}6.4$ ($-\text{OOC}-\text{CH}-\text{CH}_2$), $\delta = 4.51, 4.86, 4.92$ (hydroxyl of dextran), $\delta = 4.67$ (dextran anomeric proton), $\delta = 3.9\text{--}4.2$ ($\text{O}-\text{CH}_2-\text{C}$), $\delta = 3.98$ ($-\text{OOCCH}_2-$), $\delta = 3.14\text{--}3.69$ (dextran glucosidic protons), $\delta = 3.62$ ($-\text{CH}_2\text{OH}$), $\delta = 3.33$ ($\text{CH}-\text{O}$), $\delta = 2.9, \delta = 2.7$ ($-\text{CH}_2-\text{O}-$), $\delta = 2.25$ ($-\text{CH}_2\text{COO}-$), $\delta = 1.95$ (CH_3), $\delta = 1.61$ ($-\text{OOCCH}_2\text{CH}_2\text{CH}_2\text{CH}_2\text{OCO}-$), $\delta = 1.35$ ($-\text{CH}_2\text{CH}_2\text{CH}_2\text{COO}-$), suggesting successful synthesis of polycaprolactone-2-hydroxyethyl 2-bromoisobutyrate (PCL-HEBIB), dextran-acryloyl chloride (Dex-AC), PCL-Dex and polycaprolactone-dextran-poly(glycidyl methacrylate) (PCL-Dex-PGMA) [42–45]. The chain segment length was determined by the integrated area of the characteristic peaks at 4.67, 3.98, 2.7 and 1.95 ppm.

A series of $\text{PCL}_n\text{-Dex}_{60}$ polymers were synthesized (Fig. S1 and Table S1). We found that $\text{PCL}_{30}\text{-Dex}_{60}$ formed clear solution, implying that hydrophilic dextran was predominant in the copolymer. While $\text{PCL}_{60}\text{-Dex}_{60}$ solution showed poor stability as a small amount of sediment was observed after standing for 14 days. Further increasing PCL length, noticeable precipitation occurred to $\text{PCL}_{90}\text{-Dex}_{60}$ solution after preparation immediately. The cause lied in that the excessively long hydrophobic chain segment of PCL reduced the stability of nanoparticles. Among them, only $\text{PCL}_{45}\text{-Dex}_{60}$ formed stable suspension and no precipitation occurred even after 30 days of preparation. In order to verify the inner structure of $\text{PCL}_{45}\text{-Dex}_{60}$ assemblies from a theoretical perspective, the radius of gyration (R_g) and hydrodynamic radius (R_h) were determined. The R_g/R_h ratios can provide the information on the solution assemblies of the polymer: $R_g/R_h = 0.77$ for hard spheres, $R_g/R_h = 1$ for vesicles, and $R_g/R_h = 1.7$ for coil-like structures [37,38]. The R_h of the $\text{PCL}_{45}\text{-Dex}_{60}$ assemblies was 99.1 nm (Fig. 3a, the half of hydrodynamic diameter value is R_h). The R_g was calculated from Guinier plot (Fig. 3b, the calculation for R_g was detailed in the experimental section). It is noteworthy that the R_g/R_h value for the $\text{PCL}_{45}\text{-Dex}_{60}$ polymer assemblies was ~ 1.0 , suggesting the formation of vesicles.

Fig. 3c–i showed the size and morphology of legumain-induced cross-linked nanoparticles as measured by dynamic light scattering (DLS) and transmission electron microscopy (TEM). Before addition of legumain, the hydrodynamic diameter of the nanovesicles was in the range of 198–203 nm (Fig. 3c and Table S2). With increasing the molar ratios of $[\text{Vesicle}_{\text{AK}}]/[\text{Vesicle}_{\text{CABT}}]$ from 1:1 to 7:1, the size of the formed vesicles increased from 800 nm to more than 4.5 μm (Fig. 3d and Table S3). While the legumain-induced cross-linked $\text{Vesicle}_{\text{PCL}_{45}\text{-Dex}_{60}\text{-PGMA}_{12}\text{-AK}}$ ($\text{Vesicle}_{\text{AK}}$) and $\text{Vesicle}_{\text{PCL}_{45}\text{-Dex}_{60}\text{-PGMA}_{12}\text{-CABT}}$ ($\text{Vesicle}_{\text{CABT}}$) exhibited core-shell and spherical vesicles structure (Fig. 3e–i). Interestingly, after crosslinking, rod-like and vortex-like large vesicles appeared. When the molar ratio increased to 5:1, the large nanovesicles further fused and rearranged to form a network structure. This similar phenomenon was found in the self-assembly process of block copolymers, as the ratio of the hydrophobic/hydrophilic segments changed, the morphology of the formed nanoparticles changed from well dispersed nanoparticles to large compound vesicles (LCVs) [46–49]. The cross-linking should occur in brain parenchymal, large nanoaggregates act as reservoir for drug release. Under conditions that mimic the intracellular environment, the cumulative release rate of DON HCl from V_{DON} was $89 \pm 3.2\%$ after 48 h. MEM HCl and INS released from the nanomedicine showed a similar kinetic profile (Fig. 4a, S2 and S13 and Table S4).

3.2. Neuroprotective effect and intracellular retention of induced cross-linked vesicles (ICV)

We further proceeded to examine the neuroprotective capacity and efflux inhibition effects of the functionalized vesicles on the SH-SY5Y

cell culture. Hence, the protective effect of drug-loaded vesicles on A β 42-induced SH-SY5Y cell injury was evaluated by cell viability via methylthiazolyl tetrazolium (MTT) assay (Fig. 4b), intracellular retention via flow cytometry (Fig. 4c) and laser confocal microscopy (Fig. 4d). Previous studies demonstrated that A β 42-injured SH-SY5Y cell can mimic subcellular organ damage and stimulate legumain overexpression [22,23,50]. The incubation time and concentration of A β 42 was determined by MTT test (Fig. S3). In this test, MV was the mixture of the V_{INS} , V_{DON} and V_{MEM} vesicles. ICV was the mixture of the V_{INS} , V_{DON} , V_{MEM} vesicles and V_{CABT} vesicles (the molar ratio of V_{AK} vesicles and V_{CABT} vesicles is 5:1), those could be induced cross-linking by over-activated legumain. The cell viability of A β 42-injured SH-SY5Y cells showed similar results over this time frame after MEM/DON/INS MV and drug co-encapsulation vesicle (MEM/DON/INS V) treatments. In contrast, the cell viability of A β 42-injured SH-SY5Y cells treated with the MEM/DON/INS ICV was very close to that of normal SH-SY5Y cells (Fig. 4b). Thus, we have reason to believe that MEM/DON/INS ICV treatment can effectively repair SH-SY5Y cell damage caused by A β 42.

In order to verify whether the best therapeutic effect of the induced cross-linked vesicles are related to the high retention rate of nanovesicles, the model drug rhodamine B (RhB) was selected to compare the differences between induced cross-linked vesicles ($^{\text{RhB}}\text{ICV}$, the mixture of $^{\text{RhB}}\text{Vesicle}_{\text{AK}}$ and V_{CABT} vesicles) and noncross-linked vesicle ($^{\text{RhB}}\text{Vesicle}_{\text{AK}}$). The SH-SY5Y cells were treated with $^{\text{RhB}}\text{Vesicle}_{\text{AK}}$ or $^{\text{RhB}}\text{ICV}$ in DMEM for 2 h, 8 h and 24 h, and intracellular fluorescence intensity was quantitatively analyzed by flow cytometry. It was shown that the intracellular fluorescence intensity increased first and then decreased with time, and reached a maximum value at 8 h. Interestingly, the intracellular fluorescence intensity of SH-SY5Y cells treated with $^{\text{RhB}}\text{ICV}$ was 7-fold higher ($p < 0.005$) than that of $^{\text{RhB}}\text{Vesicle}_{\text{AK}}$ treatment at 24 h (Fig. 4c and S4).

To further determine if the cellular uptake of the nanovesicles experienced endosome/lysosome pathway, colocalization was performed by encapsulation of RhB for lysosomal staining. Fig. 4d showed that the red fluorescence was distributed in the SH-SY5Y cells at 2 h, and then no fluorescence was observed at 24 h, suggesting the $^{\text{RhB}}\text{Vesicle}_{\text{AK}}$ could effectively cross the cell membrane and transported into endosome/lysosome, while the noncross-linked vesicle was difficult to be retained due to active efflux. By contrast, the $^{\text{RhB}}\text{ICV}$ also underwent endosome/lysosome pathway, with red fluorescence being detected in the SH-SY5Y cells internal area at 24 h, demonstrating the superior retention capacity of these vesicles. These results provided clear evidence that the legumain-induced cross-linked vesicles (ICV) had a better nerve cell retaining efficiency.

3.3. Improvement of memory ability of SAMP8 mice

We determined the improved memory function of senescence accelerated mouse prone 8 (SAMP8) after legumain-induced intelligent cross-linked nanovesicles treatment. The drug clinical standard dose was determined based on the treatment efficacy and its side effects, so each drug has its appropriate dosage. While, in large amount of the preclinical medicine literatures, the dose of medicine with different chemical design for improving the transporting and physiological barriers crossing capacity was designed to be same equivalent or approximate equivalent in the animal experiment [51–53]. And after the approximate equivalent drug administration in animal model, that the optimal medicine design system is summarized, evaluated and discussed. Furthermore, in the drugs combination treatment therapy that “cocktail” of drugs to achieve maximum benefit, how to observe the treatment efficacy, the possible treatment mechanism and the side effects of multiple drugs is a central theme. So, the combination treatment outcomes of multiple drugs were survey and analyze after the approximate equivalent drugs were administrated [54–57].

The memory ability of SAMP8 mice treated with drug-loaded vesicles was confirmed by Morris water maze (MWM) experiment after 24 days

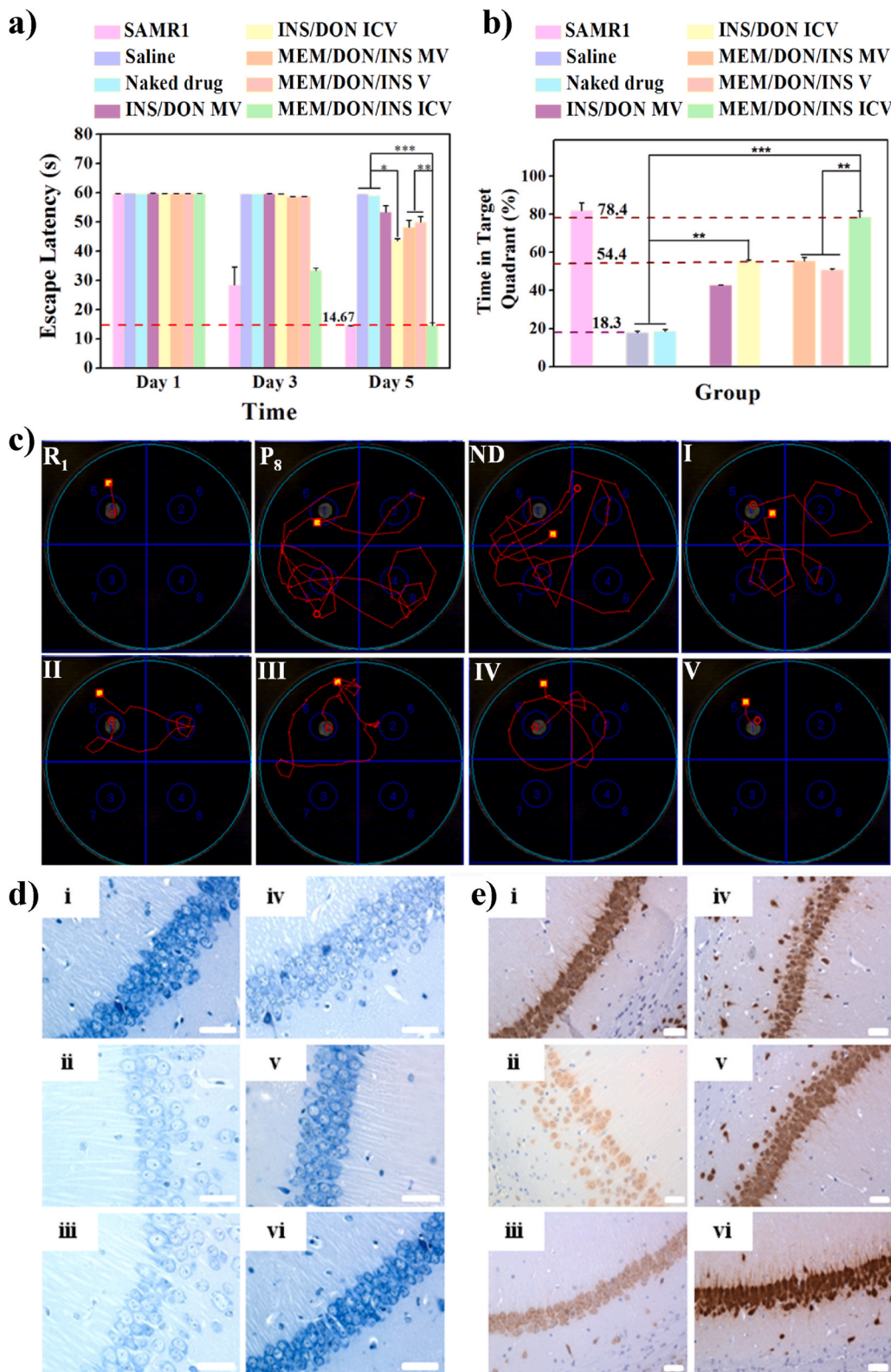


Fig. 5. MEM/DON/INS ICV treatment significantly improved the memory capacity of SAMP8 mice. a) The escape latencies of eight groups. b) The percentage (%) of time in the targeted quadrant in the eight groups during the probe trial. c) Typical motion track of each group mice on the fifth day (Yellow highlight is starting point, red empty circle is ending point, gray circle is the target platform location. III, IV, V are the motion tracks of mouse-1 of each treatment group). R₁: SAMR1, P₈: SAMP8 saline, ND: Naked drug (the mixture of MEM/DON/INS), I: DON/INS MV, II: DON/INS ICV, III: MEM/DON/INS MV, IV: MEM/DON/INS V, V: MEM/DON/INS ICV. d) Nissl staining (Scale bar, 50 μm) and e) Neun staining of nerve cells (Scale bar, 50 μm). i: SAMR1, ii: SAMP8 saline, iii: naked drug (the mixture of MEM/DON/INS), iv: MEM/DON/INS MV, v: MEM/DON/INS V, vi: MEM/DON/INS ICV. The mean ± SD is shown. *p < 0.05 and **p < 0.01 (n = 6) versus control.

treatment. The memory ability of SAMP8 mice treated with saline or naked drugs was not improved, and the animals unable to find platform within the specified time (60 s). The memory ability of SAMP8 mice achieved a certain degree of recovery via MEM/DON/INS MV and MEM/DON/INS V treatments, and their escape latency was about 50 s (Fig. 5a and c, S5 and S14–16). Comparatively, the mice with MEM/

DON/INS ICV treatment were able to travel shorter distances to reach the platform location, showing shortest escape latencies (~14 s, close to senescence-accelerated mouse resistant 1 (SAMR1) mice) relative to other treatment mice. Likewise, only MEM/DON/INS ICV treatment mice could accurately remember the platform location and exhibited a persistent memory for the target quadrant during a probe trial (Fig. 5b).

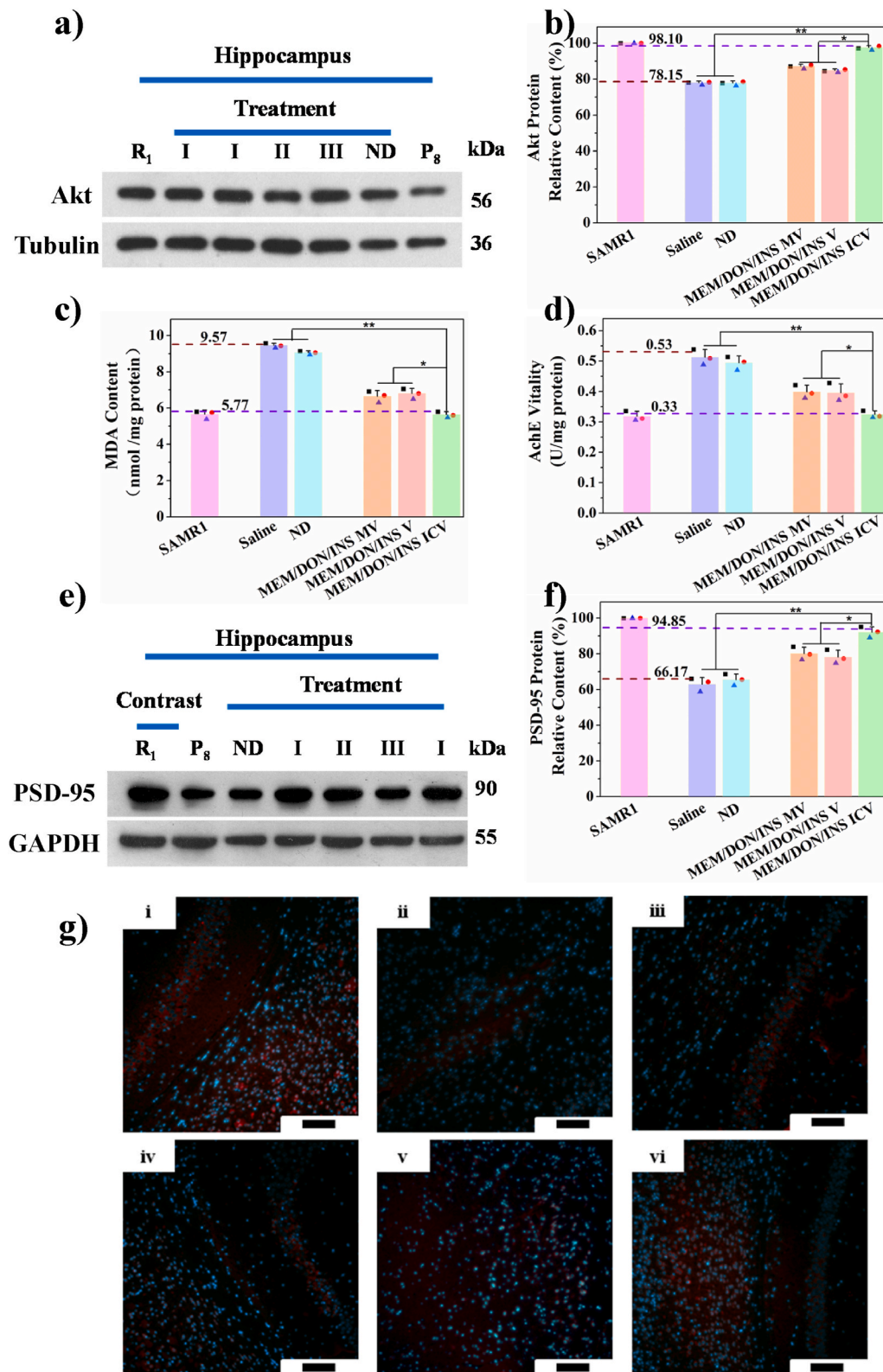


Fig. 6. MEM/DON/INS ICV treatment restored glucose metabolism and synaptic function-related. a) Western blot and b) Relative content of Akt protein. c) MDA content test and d) AchE vitality test. e) Western blot and f) Relative content of PSD-95 protein. g) Hippocampus immunohistochemistry of mice, DAPI (blue), PSD-95 protein (red) and Akt protein (green) (Scale bar, 50 μ m). i: SAMP8, ii: mixture of MEM/DON/INS, iii: Naked drug (the mixture of MEM/DON/INS), iv: MEM/DON/INS MV, v: MEM/DON/INS V, vi: MEM/DON/INS ICV. The mean \pm SD is shown. * $p < 0.05$ and ** $p < 0.01$ ($n = 3$) versus control.

In addition, similar swimming speeds (~ 10 cm/s, Fig. S6) indicated that differences in memory abilities were not caused by vision or motor dysfunction. Since the memory of mice changed over time with treatment, biomarker staining in hippocampus, like active nissl substance and nuclear protein (NeuN) were detected. The main function of the nissl substance is to synthesize the substances required for organelle

renewal, which serve as markers of neuronal functional status [58]. The severe cell damage, large cell debris and less nissl substance were revealed in hippocampus slices by immunohistochemical analysis from SAMP8 mice treated with saline and naked drug (Fig. 5d). The nerve cells in the hippocampus arranged regularly, and the cytoplasmic nissl content increased after MEM/DON/INS MV treatment. More

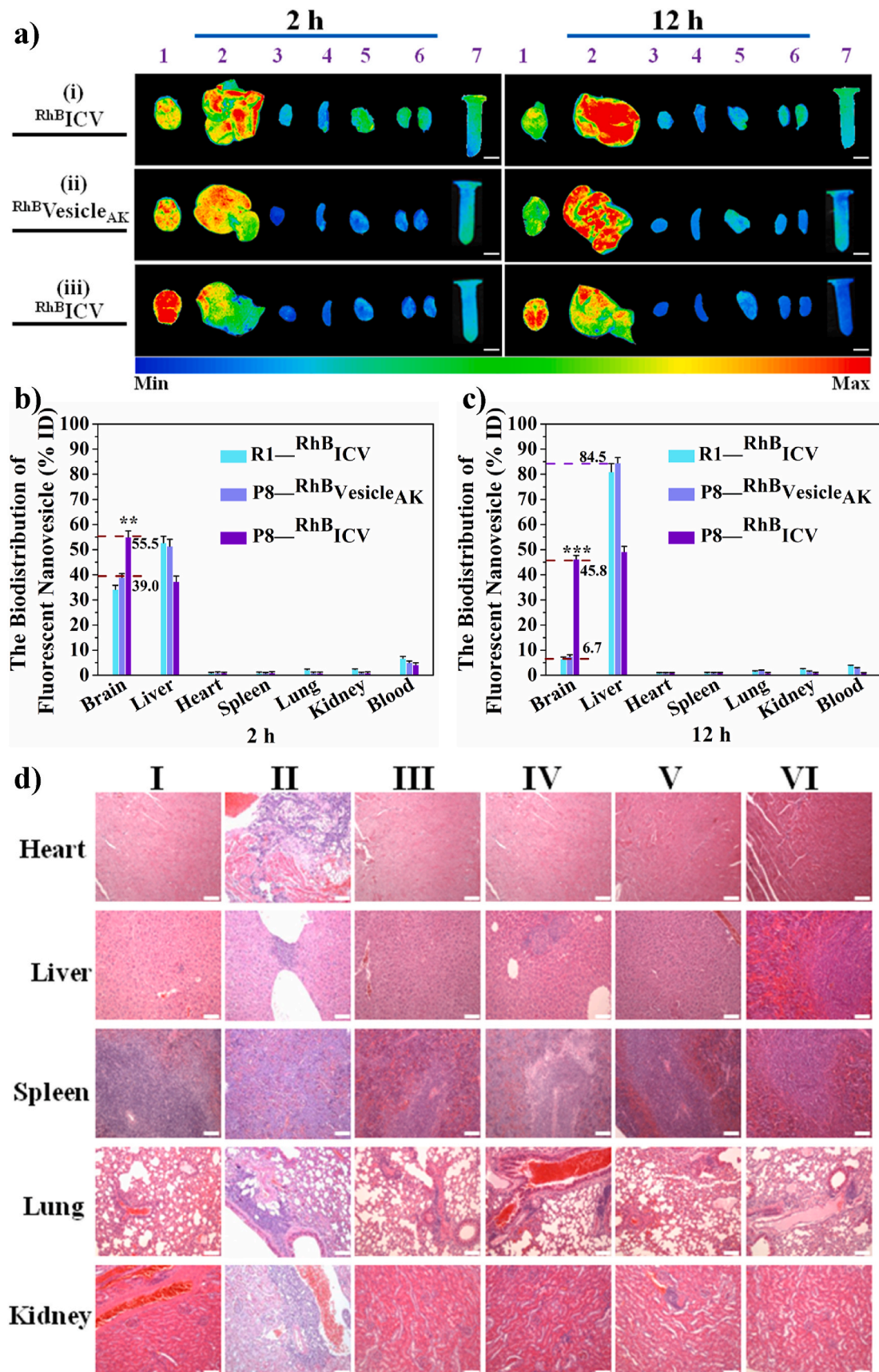


Fig. 7. Induced cross-linked nanovesicles can effectively improve the drug brain retention and non-toxic to organs. **a)** Ex vivo fluorescence images of SAMR1 (i) or SAMP8 (ii and iii) mice (Scale bar, 5 mm) and **b)** The biodistribution of fluorescent nanovesicles after treatment with RhB_{Vesicle_{AK}} or RhB_{ICV} for 2 and **c)** 12 h. 1: Brain, 2: Liver, 3: Heart, 4: Spleen, 5: Lung, 6: Kidney, 7: Blood. **d)** H&E staining (Scale bar, 50 μm). I: SAMR1, II: Saline, III: Naked drug (the mixture of MEM/DON/INS), IV: MEM/DON/INS MV, V: MEM/DON/INS V, VI: MEM/DON/INS ICV. The mean ± SD is shown. **p < 0.01, and ***p < 0.005 (n = 3) versus control.

importantly, a complete contour of hippocampus CA1 region and tightly arranged neurons could be observed, and no obvious cell damage or cell debris, a large amount of active nissl substance contained in cytoplasm after treating with MEM/DON/INS ICV. NeuN, a neuronal specific nuclear protein in vertebrates, was used to detect the number and distribution of neurons. The number of NeuN positive cells in SAMP8 mice hippocampus after MEM/DON/INS ICV treatment was 1642 ± 129 , approaching to those of SAMR1 group (1663 ± 88). This value was 2 times higher than that of MEM/DON/INS MV group and 8 times higher than that of saline group (Fig. 5e and S7). The results indicated that neuronal damage in the brain of SAMP8 mice could be efficiently repaired via MEM/DON/INS ICV treatment.

3.4. Improvement of mitochondrial function and recovery of synaptic plasticity by induced cross-linked vesicles

In order to study the contribution of combination therapy to sub-cellular organelle repair from the perspective of signaling pathways, some of the mitochondrial and synaptic function-related biomarkers were examined, including protein kinase B (Akt), reactive oxygen species (ROS), postsynaptic density-95 (PSD-95), and acetyl cholinesterase (AChE). Among them, Akt protein was an important biomarker in PI3K/Akt signaling pathway, and this pathway played a crucial role in glucose metabolism. The activation Akt protein was stimulated by insulin drug, which could promote the transition of glucose transporter (GLUT) to the cell membrane, enhance the uptake and utilization of glucose in the cell, maintain the stability of the energy metabolism cycle, facilitate the normalization of mitochondrial function, and reduce ROS content [34, 35]. The Akt protein content of MEM/DON/INS ICV treatment mice was 29% higher than that of saline or naked drug treatment mice (Fig. 6a and b). While the ROS content from MEM/DON/INS ICV treatment mice was close to that of the SAMR1 mice (Fig. 6c). Previous studies suggested that AChE and PSD-95 protein played a key role in synaptic function, and AChE disrupted the stability of intersynaptic signaling by hydrolyzing acetylcholine to choline and acetic acid. AChE inhibitor-donepezil hydrochloride could effectively reduce the activity of acetylcholinesterase and maintain the stability of synaptic signals [33]. PSD-95 protein was a postsynaptic membrane compact that mainly formed a signal complex to regulate synaptic plasticity by binding different receptors. Post-synaptic membrane compact protectant-memantine hydrochloride (MEM HCl) could effectively attenuate the excitatory amino acid toxicity, and prevented post-synaptic membrane damage caused by Ca^{2+} influx [32]. In comparison with the other treatment groups, the MEM/DON/INS ICV treatment group showed the lowest AChE activity (Fig. 6d) and the highest PSD-95 content (Fig. 6e and f) in the hippocampus of SAMP8 mice. These values were close to those of SAMR1 mice, suggesting the pivotal role of MEM/DON/INS ICV therapy in repairing synaptic function damage. The immunofluorescence showed approximate results. The Akt protein (green fluorescence) and PSD-95 protein (red fluorescence) fluorescence signal intensity was enhanced in the hippocampus of MEM/DON/INS ICV treatment SAMP8 mice, in which the green fluorescence signal was overlapped with the blue fluorescence (nuclear) signal, suggesting widely distributed of Akt protein in cells (Fig. 6g). Based on the above analyses, it is reasonable to consider that the PI3K/Akt signaling pathway, cholinergic signaling pathway and excitatory amino acid signaling pathway play a vital role in the combination therapy of AD.

3.5. Brain retention

To further investigate the link between improvement of memory ability and brain retention of the intelligent drug-loaded vesicles, we used LC-MS and ex vivo tissue imaging to study the intracerebral retention. Previous studies demonstrated that the brain barrier influx and efflux of nanoparticles occurred simultaneously after 1–2 h [15,17, 21]. With the passage of time, the efflux effect gradually dominated, and

the brain retention rate of nanoparticles reached the lowest value after 6 h. The biodistribution of $\text{RhB}^{\text{Vesicle}}_{\text{AK}}$ and RhB^{ICV} vesicles at 2 h and 12 h share a common feature, that is, the brain and liver total retention constituted more than 91%, and the heart, spleen, lung, kidney and the blood retention make up was less than 9% (Fig. 7a–c). The data indicated that the nanovesicle brain accumulated efficiency depend on the combined effect of influx and efflux behavior of brain. The gap between the well-designed legumain responsive RhB^{ICV} vesicle and $\text{RhB}^{\text{Vesicle}}_{\text{AK}}$ control nanovesicles was immense. The biodistribution of $\text{RhB}^{\text{Vesicle}}_{\text{AK}}$ fluorescent nanovesicles in the brain was $39.0 \pm 1.0\%$, as similar as SAMR1 group, after nasal administration 2 h, while the percentage of the RhB^{ICV} fluorescent nanovesicles in the brain was $55.5 \pm 1.4\%$. Yet the awareness of the tremendous differences between $\text{RhB}^{\text{Vesicle}}_{\text{AK}}$ and RhB^{ICV} in the administration 12 h biodistribution data, the fluorescence signal of RhB^{ICV} group was $45.8 \pm 0.9\%$, which was ~ 6.84 -fold higher than that of $\text{RhB}^{\text{Vesicle}}_{\text{AK}}$ group. As a supplement evidence, the quantitative analysis by HPLC-MS shown that the DON target brain retention efficiency of the MEM/DON/INS ICV group was about $26.38 \pm 0.36\%$ ID/mg at 12 h, which was about 17.0-fold higher than that of the MEM/DON/INS MV group (Fig. S8 and S9). Additionally, hemolysis assays demonstrated no hemolysis for MEM/DON/INS MV or MEM/DON/INS ICV and the hemolysis ratio was lower than 1% (Fig. S10). Cerebral thrombosis or red blood cell aggregation did not occur (Fig. S11). MEM/DON/INS MV or MEM/DON/INS ICV did not have any toxic effect on liver and kidney functions and had no obvious toxicity to heart, spleen and lung of animals (Fig. 7d and S12).

4. Conclusion

We have now demonstrated that high drug-retaining smart pathological signal-triggered cross-linked vesicles (MEM/DON/INS ICV) with both synaptic and mitochondrial repair functions are necessary and sufficient to improve memory capacity of the SAMP8 mice. Mechanistically, these novel nanovesicles can enhance brain retention of INS, MEM HCl and DON HCl, acting on the PI3K/Akt pathway, the excitatory amino acid pathway and the cholinergic pathway, respectively. More importantly, these smart nanovesicles promote the balance of energy metabolism, and prevent synaptic damage, which in turn protects neuronal cells and ensures the unobstructed transmission of signals between neurons. These findings provide not only a basis for the combined treatment of AD, but also the possibility of high intracerebral retention of the drug for other disease, indicating the potential importance of this intelligent drug delivery system.

Declaration of competing interest

The authors declare that they have no known competing financial interests or personal relationships that could have appeared to influence the work reported in this paper.

CRediT authorship contribution statement

Fuxin Jiang: Methodology, Verification, Formal analysis, Investigation, Data curation, Writing - original draft, Visualization. **Jian Ren:** Resources, Methodology. **Yachai Gao:** Data curation. **Jinna Wang:** Conceptualization, Writing - review & editing, Supervision, Project administration, Data curation. **Yiping Zhao:** Conceptualization, Writing - review & editing, Supervision, Project administration.

Acknowledgements

This work was financially sponsored by the National Natural Science Foundation of China (Nos. 51773152), the Science and Technology Plans of Tianjin (15JCYBJC17900), and the Natural Science Foundation of Tianjin (18JCYBJC17500).

Appendix A. Supplementary data

Supplementary data related to this article can be found at <https://doi.org/10.1016/j.bioactmat.2020.11.024>.

References

- J. Gaugler, B. James, T. Johnson, A. Marin, J. Weuve, A. Alzheimer's, Alzheimer's disease facts and figures, *Alzheimers Dement* 15 (2019) 321–387.
- Y. Chen, L. Liu, Modern methods for delivery of drugs across the blood-brain barrier, *Adv. Drug Deliv. Rev.* 64 (2012) 640–665.
- K. Kingwell, Drug delivery: new targets for drug delivery across the BBB, *Nat. Rev. Drug Discov.* 15 (2016) 84–85.
- C. Saraiva, C. Praca, R. Ferreira, T. Santos, L. Ferreira, L. Bernardino, Nanoparticle-mediated brain drug delivery: overcoming blood-brain barrier to treat neurodegenerative diseases, *J. Contr. Release* 235 (2016) 34–47.
- W.M.C.S.F. Pardridge, blood-brain barrier, and brain drug delivery, *Expet Opin. Drug Deliv.* 13 (2016) 963–975.
- S. Krol, R. Macrez, F. Docagne, G. Defer, S. Laurent, M. Rahman, M.J. Hajipour, P. G. Kehoe, M. Mahmoudi, Therapeutic benefits from nanoparticles: the potential significance of nanoscience in diseases with compromise to the blood brain barrier, *Chem. Rev.* 113 (2013) 1877–1903.
- X. Yi, D.S. Manickam, A. Brynskikh, A.V. Kabanov, Agile delivery of protein therapeutics to CNS, *J. Contr. Release* 190 (2014) 637–663.
- T.-H. Kim, C.-H. Yea, S.-T.D. Chueng, P.T.-T. Yin, B. Conley, K. Dardir, Y. Pak, G. Y. Jung, J.-W. Choi, K.-B. Lee, Large-scale nanoelectrode arrays to monitor the dopaminergic differentiation of human neural stem cells, *Adv. Mater.* 27 (2015) 6356–6362.
- T. Yin, L. Yang, Y. Liu, X. Zhou, J. Sun, J. Liu, Sialic acid (SA)-modified selenium nanoparticles coated with a high blood-brain barrier permeability peptide-B6 peptide for potential use in Alzheimer's disease, *Acta Biomater.* 25 (2015) 172–183.
- W.A. Banks, From blood-brain barrier to blood-brain interface: new opportunities for CNS drug delivery, *Nat. Rev. Drug Discov.* 15 (2016) 275–292.
- Y. Zhou, Z. Peng, E.S. Seven, R.M. Leblanc, Crossing the blood-brain barrier with nanoparticles, *J. Contr. Release* 270 (2018) 290–303.
- W. Loscher, H. Potschka, Role of drug efflux transporters in the brain for drug disposition and treatment of brain diseases, *Prog. Neurobiol.* 76 (2005) 22–76.
- X. Hu, F.F. Yang, Y.H. Liao, L. Li, L. Zhang, Cholesterol-PEG comodified poly (N-butyl) cyanoacrylate nanoparticles for brain delivery: in vitro and in vivo evaluations, *Drug Deliv.* 24 (2017) 121–132.
- X.Y. Zheng, C. Zhang, Q. Guo, X. Wan, X.Y. Shao, Q.F. Liu, Q.Z. Zhang, Dual-functional nanoparticles for precise drug delivery to Alzheimer's disease lesions: targeting mechanisms, pharmacodynamics and safety, *Int. J. Pharm.* 525 (2017) 237–248.
- N. Ahmad, R. Ahmad, A.A. Naqvi, M.A. Alam, M. Ashfaq, M. Samim, Z. Iqbal, F. J. Ahmad, Rutin-encapsulated chitosan nanoparticles targeted to the brain in the treatment of Cerebral Ischemia, *Int. J. Biol. Macromol.* 91 (2016) 640–655.
- T. Chen, C.W. Li, Y. Li, X. Yi, R.B. Wang, S.M.Y. Lee, Y. Zheng, Small-sized mPEG PLGA nanoparticles of schisantherin A with sustained release for enhanced brain uptake and anti-parkinsonian activity, *ACS Appl. Mater. Interfaces* 9 (2017) 9516–9527.
- C.S. He, P. Cai, J. Li, T. Zhang, L. Lin, A.Z. Abbasi, J.T. Henderson, A.M. Rauth, X. Y. Wu, Blood-brain barrier-penetrating amphiphilic polymer nanoparticles deliver docetaxel for the treatment of brain metastases of triple negative breast cancer, *J. Contr. Release* 246 (2017) 98–109.
- H.L. Wong, X.Y. Wu, R. Bendayan, Nanotechnological advances for the delivery of CNS therapeutics, *Adv. Drug Deliv. Rev.* 64 (2012) 686–700.
- D. Ye, M.N. Raghnaill, M. Bramini, E. Mahon, C. Aberg, A. Salvati, K.A. Dawson, Nanoparticle accumulation and transcytosis in brain endothelial cell layers, *Nanoscale* 5 (2013) 11153–11165.
- P.K. Pandey, A.K. Sharma, S. Rani, G. Mishra, G. Kandasamy, A.K. Patra, M. Rana, A.K. Sharma, A.K. Yadav, U. Gupta, MCM-41 nanoparticles for brain delivery: better choline-esterase and amyloid formation inhibition with improved kinetics, *ACS Biomater. Sci. Eng.* 4 (2018) 2860–2869.
- A. Cano, M. Ettchetto, J.H. Chang, E. Barroso, M. Espina, B.A. Kuhne, M. Barenys, C. Auladell, J. Folch, E.B. Souto, A. Camins, P. Turowski, M.L. Garcia, Dual-drug loaded nanoparticles of Epigallocatechin-3-gallate (EGCG)/Ascorbic acid enhance therapeutic efficacy of EGCG in a APPsw/PS1dE9 Alzheimer's disease mice model, *J. Contr. Release* 301 (2019) 62–75.
- T.K. Chen, W. Liu, S. Xiong, D.L. Li, S.H. Fang, Z.F. Wu, Q. Wang, X. Chen, Nanoparticles mediating the sustained puerarin release facilitate improved brain delivery to treat Parkinson's disease, *ACS Appl. Mater. Interfaces* 11 (2019) 45276–45289.
- F. Sousa, H.K. Dhaliwal, F. Gattacceca, B. Sarmento, M.M. Amiji, Enhanced anti-angiogenic effects of bevacizumab in glioblastoma treatment upon intranasal administration in polymeric nanoparticles, *J. Contr. Release* 309 (2019) 37–47.
- X. Gu, Q.X. Song, Q. Zhang, M. Huang, M.N. Zheng, J. Chen, D. Wei, J. Chen, X. B. Wei, H.Z. Chen, G. Zheng, X.L. Gao, Clearance of two organic nanoparticles from the brain via the paravascular pathway, *J. Contr. Release* 322 (2020) 31–41.
- Z.T. Zhang, M.K. Song, X. Liu, S.S. Kang, T.S. Kwon, D.M. Duong, N.T. Seyfried, W. T. Hu, Z.X. Liu, J.Z. Wang, L.M. Cheng, Y.E. Sun, S.P. Yu, A.I. Levey, K.Q. Ye, Cleavage of tau by asparagine endopeptidase mediates the neurofibrillary pathology in Alzheimer's disease, *Nat. Med.* 20 (2014) 1254–1262.
- Z.T. Zhang, O. Obianyo, E. Dall, Y.H. Du, H.A. Fu, X. Liu, S.S. Kang, M.K. Song, S. P. Yu, C. Cabrele, M. Schubert, X.G. Li, J.Z. Wang, H. Brandstetter, K.Q. Ye, Inhibition of delta-secretase improves cognitive functions in mouse models of Alzheimer's disease, *Nat. Commun.* 8 (2017) 14740.
- J. Xiang, Z.H. Wang, E.H. Ahn, X. Liu, S.P. Yu, F.P. Manfredsson, I.M. Sandoval, G. Ju, S.X. Wu, K.Q. Ye, Delta-secretase-cleaved Tau antagonizes TrkB neurotrophic signalings, mediating Alzheimer's disease pathologies, *Proc. Natl. Acad. Sci. U. S. A* 116 (2019) 9094–9102.
- Z.T. Zhang, M.K. Song, X. Liu, S.S. Kang, D.M. Duong, N.T. Seyfried, X.B. Cao, L. M. Cheng, Y.E. Sun, S.P. Yu, J.P. Jia, A.I. Levey, K.Q. Ye, Delta-secretase cleaves amyloid precursor protein and regulates the pathogenesis in Alzheimer's disease, *Nat. Commun.* 6 (2015) 8762.
- S.B. Ruan, C. Hu, X. Tang, X.L. Cun, W. Xiao, K.R. Shi, Q. He, H.L. Gao, Increased gold nanoparticle retention in brain tumors by in situ enzyme-induced aggregation, *ACS Nano* 10 (2016) 10086–10098.
- S.B. Ruan, W. Xiao, C. Hu, H.J. Zhang, J.D. Rao, S.H. Wang, X. Wang, Q. He, H. L. Gao, Ligand-Mediated and enzyme-directed precise targeting and retention for the enhanced treatment of glioblastoma, *ACS Appl. Mater. Interfaces* 9 (2017) 20348–20360.
- S.B. Ruan, Q. He, H.L. Gao, Legumain-responsive functional gold nanoparticles for drug targeting delivery and treatment of subcutaneous xenograft tumor, *Acta Pharm. Sin.* 52 (2017) 1756–1762.
- S. Bleich, J. Wiltfang, J. Kornhuber, Memantine in moderate-to-severe Alzheimer's disease, *N. Engl. J. Med.* 349 (2003) 609–610.
- R. Howard, R. McShane, J. Lindsay, C. Ritchie, A. Baldwin, R. Barber, A. Burns, T. Denning, D. Findlay, C. Holmes, A. Hughes, R. Jacoby, R. Jones, R. Jones, I. McKeith, A. Macharouthu, J. O'Brien, P. Passmore, B. Sheehan, E. Juszcak, K. Katona, R. Hills, M. Knapp, C. Ballard, R. Brown, S. Banerjee, C. Onions, M. Griffin, J. Adams, R. Gray, T. Johnson, P. Bentham, P. Phillips, Donepezil and memantine for moderate-to-severe Alzheimer's disease, *N. Engl. J. Med.* 366 (2012) 893–903.
- S. Craft, L.D. Baker, T.J. Montine, S. Minoshima, G.S. Watson, A. Claxton, M. Arbuckle, M. Callaghan, E. Tsai, S.R. Plymate, P.S. Green, J. Leverenz, D. Cross, B. Gerton, Intranasal insulin therapy for alzheimer disease and amnesic mild cognitive impairment A pilot clinical trial, *Arch. Neurol.* 69 (2012) 29–38.
- A. Claxton, L.D. Baker, A. Hanson, E.H. Trittschuh, B. Cholerton, A. Morgan, M. Callaghan, M. Arbuckle, C. Behl, S. Craft, Long-acting intranasal insulin detemir improves cognition for adults with mild cognitive impairment or early-stage Alzheimer's disease dementia, *J. Alzheimers Dis.* 44 (2015) 897–906.
- N. Kamei, M. Tanaka, H. Choi, N. Okada, T. Ikeda, R. Itokazu, M. Takada-Morishita, Effect of an enhanced nose-to-brain delivery of insulin on mild and progressive memory loss in the senescence-accelerated mouse, *Mol. Pharm.* 14 (2017) 916–927.
- W. Burchard, Static and dynamic light scattering from branched polymers and biopolymers, *Adv. Polym. Sci.* 48 (1983) 1–124.
- C. Houga, J. Giermanska, S. Lecommandoux, R. Borsali, D. Taton, Y. Gnanou, J.-F. Le Meins, Micelles and polymersomes obtained by self-assembly of dextran and polystyrene based block copolymers, *Biomacromolecules* 10 (2009) 32–40.
- B. Surnar, M. Jayakannan, Triple block nanocarrier platform for synergistic cancer therapy of antagonistic drugs, *Biomacromolecules* 17 (2016) 4075–4085.
- N.U. Deshpande, M. Jayakannan, Cisplatin-stitched polysaccharide vesicles for synergistic cancer therapy of triple antagonistic drugs, *Biomacromolecules* 18 (2017) 113–126.
- N.U. Deshpande, M. Jayakannan, Biotin-tagged polysaccharide vesicular nanocarriers for receptor-mediated anticancer drug delivery in cancer cells, *Biomacromolecules* 19 (2018) 3572–3585.
- P.S. Pramod, K. Takamura, S. Chaphekar, N. Balasubramanian, M. Jayakannan, Dextran vesicular carriers for dual encapsulation of hydrophilic and hydrophobic molecules and delivery into cells, *Biomacromolecules* 13 (2012) 3627–3640.
- D.-B. Cheng, G.-B. Qi, J.-Q. Wang, Y. Gong, F.-H. Liu, H. Yu, Z.-Y. Qiao, H. Wang, In situ monitoring intracellular structural change of nanovehicles through photoacoustic signals based on phenylboronate-linked RGD-dextran/purpurin 18 conjugates, *Biomacromolecules* 18 (2017) 1249–1258.
- Y. Sun, H. Hu, B. Yu, F.-J. Xu, PGMA-based cationic nanoparticles with polyhydric iodine units for advanced gene vectors, *Bioconjugate Chem.* 27 (2016) 2744–2754.
- X. Wang, W. Yun, W. Jiang, D. Wang, L. Zhang, J. Tang, An amphiphilic non-viral gene vector prepared by a combination of enzymatic atom transfer radical polymerization and enzymatic ring-opening polymerization, *RSC Adv.* 7 (2017) 9926–9932.
- A. Palanisamy, Q. Guo, Large compound vesicles from amphiphilic block copolymer/rigid-rod conjugated polymer complexes, *J. Phys. Chem. B* 118 (2014) 12796–12803.
- R. Vyhalkova, A.H.E. Mueller, A. Eisenberg, Control of morphology and corona composition in aggregates of mixtures of PS-b-PAA and PS-b-P4VP diblock copolymers: effects of solvent, water content, and mixture composition, *Langmuir* 30 (2014) 13152–13163.
- Y. Wu, S. Liu, Y. Tao, C. Ma, Y. Zhang, J. Xu, Y. Wei, New strategy for controlled release of drugs. Potential pinpoint targeting with multiresponsive tetraaniline diblock polymer vesicles: site-directed burst release with voltage, *ACS Appl. Mater. Interfaces* 6 (2014) 1470–1480.
- X. Cheng, Y. Jin, B. Fan, R. Qi, H. Li, W. Fan, Self-assembly of polyurethane phosphate ester with phospholipid-like structures: spherical, worm-like micelles, vesicles, and large compound vesicles, *ACS Macro Lett.* 5 (2016) 238–243.
- E. Siczekowski, C. Lehner, P.F. Ambros, M. Hohenegger, Double impact on p-glycoprotein by statins enhances doxorubicin cytotoxicity in human neuroblastoma cells, *Int. J. Canc.* 126 (2010) 2025–2035.

- [51] Y.W. Cong, H.H. Xiao, H.J. Xiong, Z.G. Wang, J.X. Ding, C. Li, X.S. Chen, X. J. Liang, D.F. Zhou, Y.B. Huang, Dual drug backbone shattering polymeric theranostic nanomedicine for synergistic eradication of patient-derived lung cancer, *Adv. Mater.* 30 (2018) 1706220.
- [52] X.L. Hu, S.D. Zhai, G.H. Liu, D. Xing, H.J. Liang, S.Y. Liu, Concurrent drug unplugging and permeabilization of polyprodrug-gated crosslinked vesicles for cancer combination chemotherapy, *Adv. Mater.* 30 (2018) 1706307.
- [53] L. Zhang, Y. Zhang, Y.N. Xue, Y. Wu, Q.Q. Wang, L.J. Xue, Z.G. Su, C. Zhang, Transforming weakness into strength: photothermal-therapy-induced inflammation enhanced cytopharmaceutical chemotherapy as a combination anticancer treatment, *Adv. Mater.* 31 (2019) 1805936.
- [54] M.B. Zheng, C.X. Yue, Y.F. Ma, P. Gong, P.F. Zhao, C.F. Zheng, Z.H. Sheng, P. F. Zhang, Z.H. Wang, L.T. Cai, Single-step assembly of DOX/ICG loaded lipid-polymer nanoparticles for highly effective chemo-photothermal combination therapy, *ACS Nano* 7 (2013) 2056–2067.
- [55] H. Hu, C. Xiao, H.L. Wu, Y.H. Li, Q. Zhou, Y.X. Tang, C. Yu, X.L. Yang, Z.F. Li, Nanocolloidosomes with selective drug release for active tumor-targeted imaging-guided photothermal/chemo combination therapy, *ACS Appl. Mater. Interfaces* 9 (2017) 42225–42238.
- [56] H.Q. Wu, H.J. Jin, C. Wang, Z.H. Zhang, H.Y. Ruan, L.Y. Sun, C. Yang, Y.J. Li, W. X. Qin, C.C. Wang, Synergistic cisplatin/doxorubicin combination chemotherapy for multidrug-resistant cancer via polymeric nanogels targeting delivery, *ACS Appl. Mater. Interfaces* 9 (2017) 9426–9436.
- [57] L.Q. Peng, X. Mei, J. He, J.K. Xu, W.K. Zhang, R.Z. Liang, M. Wei, D.G. Evans, X. Duan, Monolayer nanosheets with an extremely high drug loading toward controlled delivery and cancer theranostics, *Adv. Mater.* 30 (2018) 1707389.
- [58] A. Kadar, G. Wittmann, Z. Liposits, C. Fekete, Improved method for combination of immunocytochemistry and Nissl staining, *J. Neurosci. Methods* 184 (2009) 115–118.